Photoinduced Formation of a Cryptand from a Coronand: An Unexpected Switch in Cation Binding Affinity

Gordon McSkimming,[a] James H. R. Tucker,*[a] Henri Bouas-Laurent,[b] Jean-Pierre Desvergne,*[b] Simon J. Coles,[c] Michael B. Hursthouse,[c] and Mark E. Light[c]

Abstract: Aza-crown ethers **2** and **3** with anthracene-containing pendant arms have been synthesised and characterised. Both compounds bind Group 1 metal cations in solution, forming complexes of 1:1 stoichiometry. The properties of compound **2** and its complexes have been studied by a range of techniques, including NMR, UV and fluorescence spectroscopy and X-ray crystallography. The pendant arms can adopt either a *cis* or a *trans* geometry, the *cis* geometry favoured with larger cations. The geometry of the complex affects the fluorescence properties of the system, with larger cations giving higher excimer/monomer ratios. Upon irradiation at $\lambda > 300$ nm, coronand **2** forms the cryptand **5** through a reversible intramolecular [4π+4π] cycloaddition reaction. The rates of the forward and reverse reactions of this photochromic process are cation dependent; in particular the rate of the thermal reverse reaction is decreased by smaller cations and increased by larger cations, especially Rb^+. The metal binding constants in methanol for **2** and **5** have been determined, revealing that the cryptand **5** binds Na^+ and Rb^+ more weakly than crown ether **2** by over two orders of magnitude.

Keywords: crown compounds · host–guest systems · molecular devices · photochromism · photoswitches

Introduction

Photochromic molecules, compounds that interconvert between one form and another upon the action of light, are expected to play an important role in the development of novel materials that can process optical information for data storage and display applications.[1] There is ongoing interest in adding extra functionality and control to photochromic systems so that a compound, in addition to responding to light, is affected by a separate stimulus, for example, by metal complexation[2] or by electron transfer.[3] In this way, *gated photochromic systems* (terminology given by Irie[1b,e]) can be developed. One advantage that such systems offer is that there is the possibility of one or both photostates being temporarily "locked" so that "written" information can be "read-out" easily or stored (e.g., by temporarily preventing the reverse process). Anthracenes, which undergo a well-characterised and thermally reversible [4π+4π] photodimerisation reaction, have been utilised by us[4] and by others[5] in a number of functional photochromic systems over the past two decades. Perhaps the earliest example of a compound exhibiting gated photochromism, **1**,[4a] contained two anthracenes linked by an ethyleneoxy chain for binding s-block cations. Photocyclisation in the presence of $LiClO_4$ stabilised the photoproduct to such an extent that the thermal reverse reaction did not occur in nonpolar solvents. We have subsequently extended this system by incorporating bipyridine groups to enable both d-block and s-block metals to be complexed.[4b] Here we report the effect of complexation on a crown ether/cryptand photochromic system in which light induces an unexpected change in metal-cation binding affinity. Initial results of this work were published previously.[4c]

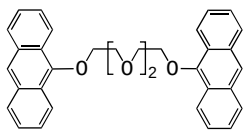

1

[a] Dr. J. H. R. Tucker, G. McSkimming
School of Chemistry, University of Exeter
Stocker Road, Exeter, EX4 4QD (UK)
Fax (+44) 1392-263-434
E-mail: j.h.r.tucker@exeter.ac.uk

[b] Dr. J.-P. Desvergne, Prof. H. Bouas-Laurent
Photochimie Organique, LCOO, CNRS UMR 5802
Université Bordeaux 1, 33405 Talence (France)
Fax (+33) 5-56-84-66-46
E-mail: jp.desvergne@lcoo.u-bordeaux.fr

[c] Dr. S. J. Coles, Prof. M. B. Hursthouse, Dr. M. E. Light
EPSRC National Crystallography Service
Department of Chemistry, University of Southampton
Highfield, Southampton, SO17 1BJ (UK)

Supporting information for this article is available on the WWW under http://www.wiley-vch.de/home/chemistry/ or from the author.

  0947-6539/02/0815-3331 $ 20.00+.50/0

Results and Discussion

Synthesis: Compounds **2** and **3** were first prepared using the pathway outlined in Scheme 1 (Route 1 in Experimental Section). 9-(2-Chloroethoxy)anthracene and 9-(2-bromoethoxy)anthracene were prepared from the reaction between anthrone and the corresponding alcohol under Dean–Stark conditions as employed by Pirkle and Finn.[6] These were subsequently converted to their more reactive iodo counterparts by refluxing with sodium iodide in acetone.

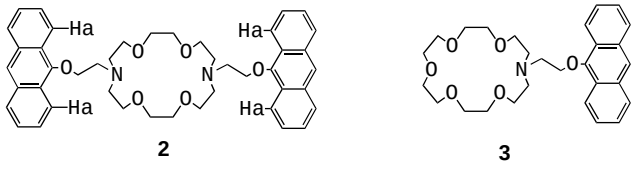

2 **3**

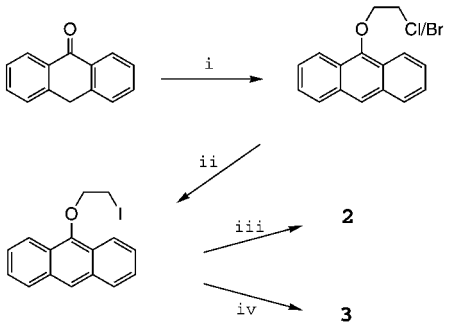

Scheme 1. Synthetic pathway (Route 1) for compounds **2** and **3**. Reagents and conditions: i) $ClCH_2CH_2OH$ or $BrCH_2CH_2OH$, H_2SO_4, benzene reflux 48 h; ii) NaI, acetone reflux, 48 h; iii) 0.45 equiv diaza-[18]crown-6, $i Pr_2EtN$ (excess), MeCN reflux 72 h; iv) 0.9 equiv diaza-[18]crown-6, $i Pr_2EtN$ (excess), MeCN reflux 48 h.

Ligands **2** and **3** were synthesised by the reaction between 9-(2-iodoethoxy)anthracene and the relevant aza-crown ether in acetonitrile by using $i Pr_2EtN$ as the base.[7] Diaza-[18]crown-6 was treated with 2.2 equivalents of the anthracene precursor to give **2** as an orange solid in moderate yield after column chromatography on alumina. Ligand **3** was synthesised by treating 1-aza-[18]crown-6 with 1.1 equivalents of the anthracene precursor under identical conditions. The product was obtained as a brown semisolid after chromatography on alumina. The synthesis of reference chromophore **4** has been published elsewhere.[8]

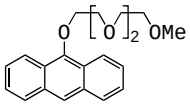

4

A separate pathway to coronand **2** was followed (Route 2 in Experimental Section), also starting from anthrone but using α-bromoethylacetate in the first step, as outlined in Scheme 2.

NMR studies: Ligand **2** forms metal complexes with Group 1 cations, as evidenced by changes to the ^1H NMR spectrum of the ligand upon addition of cations in $CDCl_3/CD_3OD$ (50:50). The expected 1:1 stoichiometry of these complexes was

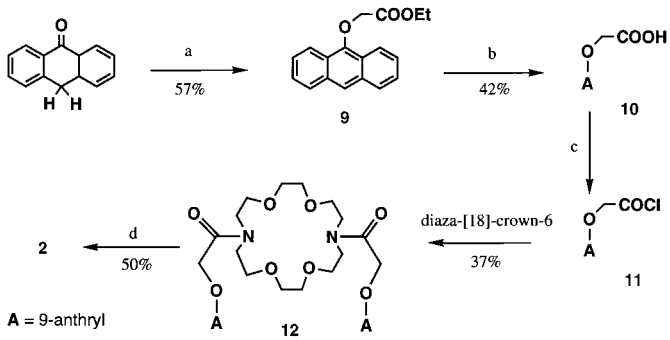

Scheme 2. Synthetic pathway (Route 2) for compound **2**. Reagents and conditions: a) $ClCH_2COOEt$, K_2CO_3, acetone; b) NaOH(aq.), EtOH; c) $(COCl)_2$, benzene; d) i) B_2H_6, THF; ii) CF_3COOH, THF, 0–40 °C; iii) $Et_4N^+OH^-$, CH_2Cl_2. Overall yield ≈10%.

confirmed by titrating an anthracenyl proton resonance (e.g., that for H_a) against molar equivalents of metal cation (see Supporting Information). A 2:1 stoichiometry of the complex with H^+ was confirmed in a similar fashion, and by X-ray studies (see below).

In principle, the complexes can adopt either a *cis* or a *trans* geometry (Figure 1). However the observation of only one set of signals upon addition of cations indicated that any exchange between free ligand and complex, as well as any interconversion between the two isomers, was fast on the NMR timescale. *Cis* and *trans* isomers have been observed in other pendant-arm diaza-crown complexes, although the preference for a particular isomer as the Group 1 cation is varied appears to depend on the particular ligand; for example, a *cis* orientation can be favoured as the Group 1 cation size decreases[9a] or increases.[10] For complexes with ligand **2**, it is clear from a range of spectroscopic studies that the latter situation is the case. For example, the NMR spectra reveal large upfield shifts in the resonances corresponding to the anthracenyl protons upon the addition of Rb^+ and Cs^+ (Figure 2), which indicates that $\pi-\pi$ interactions are present in these complexes and a *cis* orientation is favoured with these larger cations.

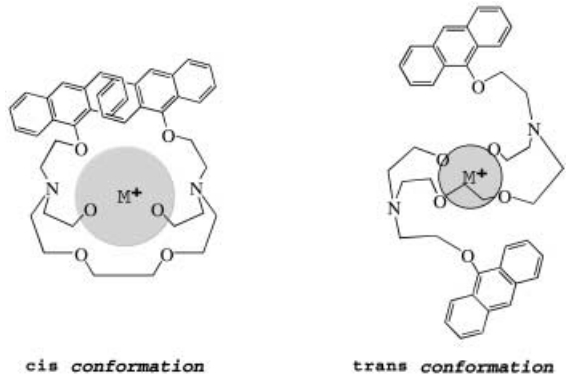

Figure 1. The complex $[\mathbf{2}{:}M]^+$ with the anthracenyl groups depicted *cis* and *trans* to one another.

As a comparison, the same study was carried out with ligand **3**; only small changes to the NMR spectrum of this ligand were observed upon the addition of cations (see

  0947-6539/02/0815-3332 $ 20.00+.50/0 *Chem. Eur. J.* **2002**, *8*, No. 15

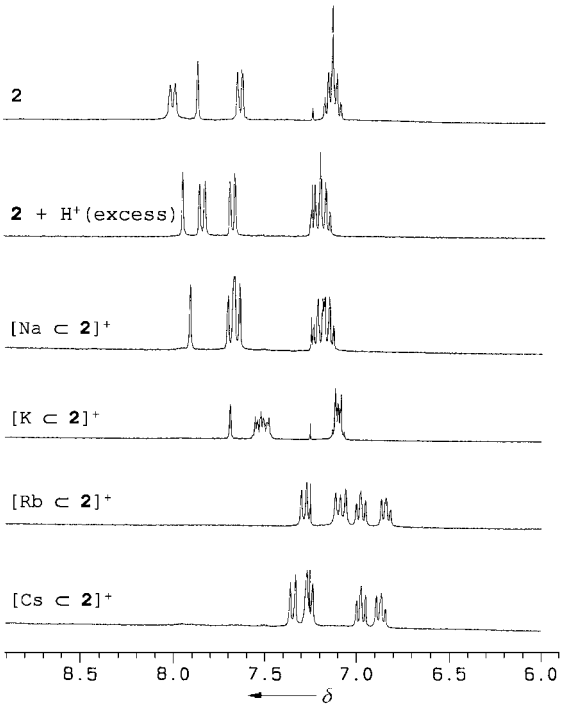

Figure 2. ^{1}H NMR spectra of **2** (aromatic region) in $CDCl_3/CD_3OD$ (50:50, 5 mM) in the absence and in the presence of protons and Group 1 metal salts (acetates).

Supporting Information). Significantly, the splitting pattern was similar for all Group 1 cations and resembled the pattern seen for the addition of smaller cations to **2**. These observations give a strong indication that the changes to the aromatic region of **2** upon the addition of larger cations are a direct result of $\pi-\pi$ and not $M^+-\pi$ interactions.

X-ray crystallographic studies: Crystals of ligand **2** suitable for X-ray crystallography were grown by diffusion of heptane into a chloroform solution over a period of one month at room temperature. The resulting structure (Figure 3) reveals the pendant arms in a *trans* conformation, as expected from NMR studies. Bond lengths and bond angles are reported in the Supporting Information. They are similar to values reported for related macrocylic compounds.[9b]

The 2:1 product of ligand **2** with H^+ was confirmed by X-ray crystallography. Crystals of the protonated form of **2** suitable for diffraction were grown by diffusion of diethyl ether into a solution of **2** with an excess of trifluoroacetic acid (CF_3CO_2H) over a period of 2 weeks. The X-ray structure of $[\mathbf{2}{:}2H]^{2+}$ (see Supporting Information) depicts two crowns and two trifluoroacetate anions, which in fact are hydrogen bonded to two other diprotonated crowns, as shown in Figure 4. It is clear that the two pendant arms of the macrocycle are in a *trans* conformation in the solid state, as found with the solution studies. Selected bond lengths and angles are shown in the Supporting Information.

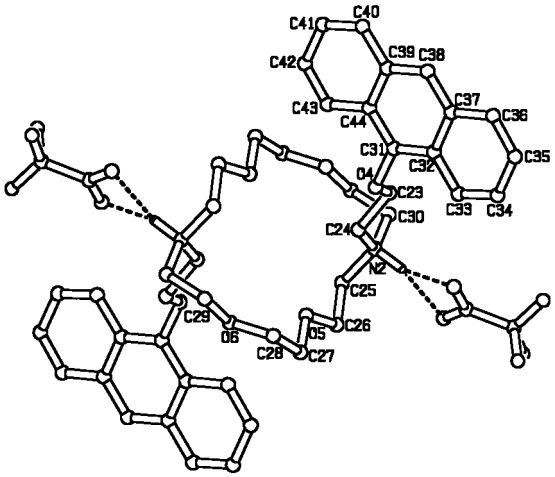

Figure 4. X-ray structure of $[\mathbf{2}{:}2H]^{2+}$ with two symmetry generated trifluoroacetate counter-anions hydrogen-bonded to one diprotonated crown ether. (See Supporting Information for a depiction of two crowns and two trifluoroacetate counter-anions to allow a complete atomic numbering scheme).

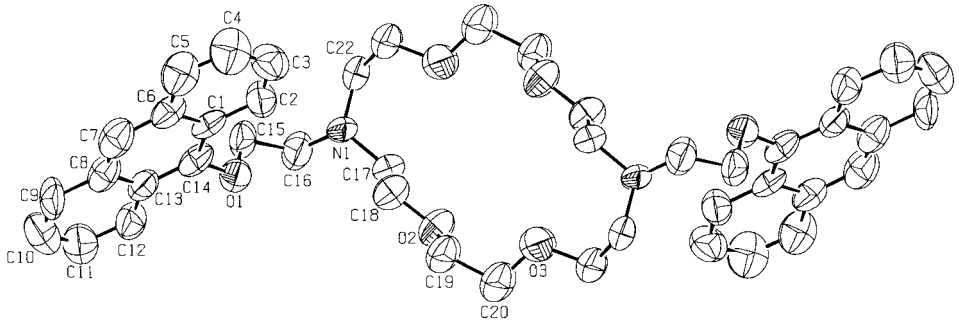

Figure 3. X-ray structure of **2** showing the atomic numbering scheme.

UV spectroscopy: The UV spectrum of ligand **2** consists of two electronic transitions: A low-energy (300–400 nm) transition band (^1L_a) and a higher energy (250–270 nm) band based on the second electronic transition of anthracene (^1B_b).[4d] Previous UV studies on bis-anthracenes have shown that the shape of the latter transition band is dependent on the degree of interaction between the two aromatic rings.[4d] Therefore, UV absorption spectra of **2** in its free form and in the presence of a variety of Group 1 cations were recorded in order to examine qualitatively the degree of interaction between the two aromatic rings with respect to cation size (Figure 5).

Results show that for a nonperturbed aromatic ring, the 256 nm component of the ^1B_b band largely predominates; conversely the 248 nm component intensity increases as a function of the degree of interaction between the two rings. The UV spectrum of **2** is therefore indicative of a mixture of *cis* and *trans* isomers. When Rb^+ or Cs^+ (and to a lesser extent K^+) were added in excess, the intensity of the 248 nm band increased, indicating an increase in the *cis/trans* ratio. When Na^+ was added in excess,

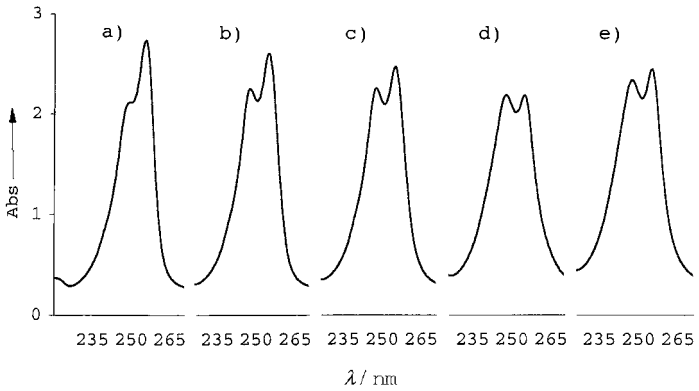

Figure 5. UV Spectra in CH_3OH (ca. 5×10^{-6} M, 20 °C) of a) compound **2**; b) **2** + $NaClO_4$ (ca. 10^{-2} M); c) **2** + $KClO_4$ (ca. 10^{-2} M); d) **2** + $RbClO_4$ (ca. 10^{-2} M); e) **2** + $CsClO_4$ (ca. 10^{-2} M).

the two parts of the ^1B_b band became more distinguished from each other and a clear separation was noted between the two components. The difference in size between the 248 and 256 nm components points to an increase in the *trans*/*cis* ratio for the Na^+ complex. A similar result was found upon the addition of excess CF_3COOH to **2**.[4c] Therefore these findings are in keeping with those found from the NMR and X-ray studies. It is also interesting to note that both NMR and UV spectroscopy indicate that $\pi-\pi$ interactions are the strongest in the Rb^+ complex.

Fluorescence spectroscopy: Ligand **2** exhibits a dual fluorescence composed of a structured part, culminating at 420 nm, assigned to the locally excited species referred to as the "monomer", and a broad and structureless red-shifted band consisting of a combination of exciplex (amine–anthracene* interaction) and excimer (anthracene–anthracene*) species. By using a suitable reference compound **4**, which is unable to form an exciplex or an intramolecular excimer (and so its emission spectrum consists purely of monomer-type emission), the shape of this red-shifted region (denoted "excimer-type"), as well as the percentage of the total emission spectrum it composes, can be deduced by subtraction of the spectra (Figure 6). Emission spectra for **2** were also recorded in the presence of a large excess (ca. 10^{-2} M) of protons (CF_3CO_2H) and Group 1 metal cations. Amongst the cations studied, Rb^+ and in particular Cs^+ give the highest excimer/monomer ratio for **2** (Figure 7, Table 1), as expected from the preferred *cis* complex geometry with these cations in the ground state. It is also clear that the shape of this excimer region differs considerably compared to the free ligand. The difference in wavelength of maximum excimer emission (540 nm for Rb^+ and 525 nm for Cs^+) also suggests that these two excimers have a different geometry, resulting from slightly different conformations of the complex.[11] The larger overlap between the aromatic nuclei is presumably experienced by the Rb^+ system, since this emits at a longer wavelength.[4d]

Table 1. Fluorescence quantum yields (Φ_{FT}) for compound **2** (ca. 5×10^{-6} M, 20 °C) and upon addition of Group 1 cations and H^+ (ca. 10^{-2} M), together with quantum yields of monomer (Φ_{FM}) and excimer-type (Φ_{FE}) emission ($\Phi_{FT}=\Phi_{FM}+\Phi_{FE}$) in degassed methanol.[a]

System	Φ_{FM}	Φ_{FE}	Φ_{FT}
2	0.051	0.019	0.07
2 + H^+	0.125	0.005	0.13
2 + Na^+	0.064	0.016	0.08
2 + K^+	0.066	0.024	0.09
2 + Rb^+	0.049	0.021	0.07
2 + Cs^+	0.057	0.033	0.09

[a] For comparison, compound **4** has $\Phi_{FT}=0.36$.

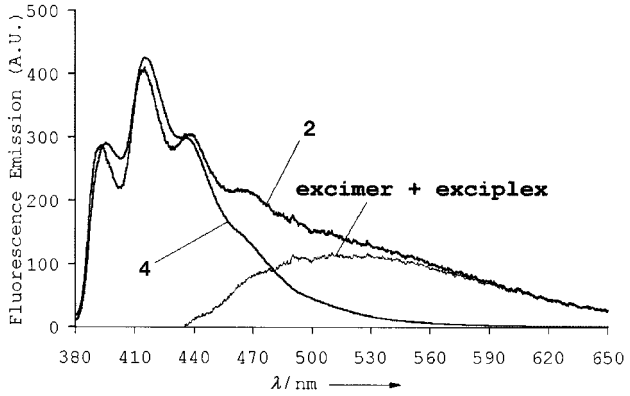

Figure 6. Corrected fluorescence emission spectra of **2** and reference chromophore **4** normalized at the first vibronic band (conc. ca. 5×10^{-6} M, $\lambda_{exc}=368$ nm, 20 °C in MeOH.

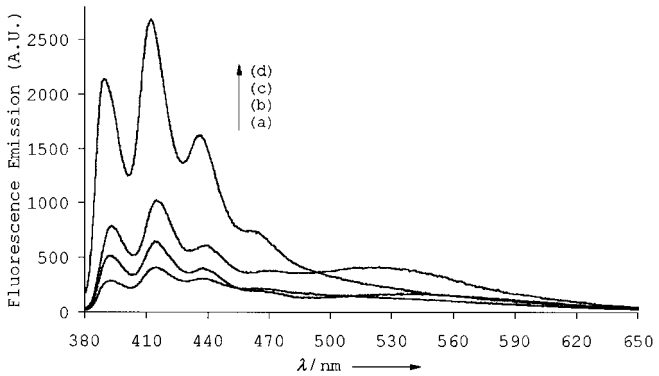

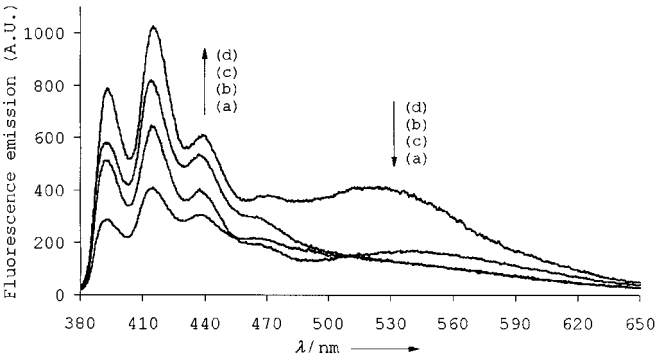

Figure 7. Corrected fluorescence emission spectra in CH_3OH (ca. 5×10^{-6} M, $\lambda_{exc}=368$ nm, 20 °C of top spectrum a) compound **2**; b) **2** + $RbClO_4$ (ca. 10^{-2} M); c) **2** + $NaClO_4$ (ca. 10^{-2} M); d) **2** + CF_3COOH and bottom spectrum a) compound **2**; b) **2** + $RbClO_4$ (ca. 10^{-2} M); c) **2** + $NaClO_4$ (ca. 10^{-2} M); d) **2** + $CsCl0_4$ (ca. 10^{-2} M).

0947-6539/02/0815-3334 $ 20.00+.50/0 *Chem. Eur. J.* **2002**, *8*, No. 15

The fluorescence quantum yields (Table 1) of **2** are not significantly affected by the addition of metal cations, although in general, a slight increase is observed. This is probably due to the cations coordinating to the emission-quenching amine nitrogen lone pairs, which reduces the quenching. This quenching diminishes even more upon protonation, as shown by the large increase in quantum yield upon the addition of CF_3COOH. The addition of H^+ is also accompanied by a clear decrease of the long wavelength excimer contribution, in keeping with the *trans* complex geometry indicated by the spectroscopic studies described above and the X-ray structure of $[\mathbf{2}{:}2\,H]^{2+}$.

Transient kinetics: The time-dependent fluorescence intensities were recorded at 400 and 550 nm, corresponding to the monomer and excimer contributions, respectively. Fluorescence emission decay at these wavelengths is well fitted by a linear combination of two exponentials, as evidenced by the χ^2 values (1.0–1.3) and other statistical parameters (see Experimental Section) both at room temperature (20 °C) and at low temperature (−50 °C), obeying Equation (1) (Tables 2 and 3).

$$I_F(t) \propto A_1 \exp(-\lambda_1 t) + A_2 \exp(-\lambda_2 t) \quad (1)$$

Table 2. Kinetic parameters ($1/\lambda$) obtained from fluorescence emission decays of **2** (ca. 5×10^{-6} M) in the absence and in the presence of metal perchlorates (ca. 10^{-2} M) at 400 nm (monomer) and 550 nm (excimer) at 20 °C in degassed MeOH.

System	A_1	$1/\lambda_1$ [ns]	A_2	$1/\lambda_2$ [ns]	$\chi^{2[a]}$
$\lambda_{obs} = 400$ nm					
2	−1.06	0.59	1.00	3.89	1.24
2 + H^+	0.16	1.87	0.49	3.78	1.04
2 + Na^+	0.40	0.70	0.57	3.91	1.05
2 + K^+	0.32	0.90	0.57	4.01	1.22
2 + Rb^+	0.63	0.76	0.45	4.92	1.20
2 + Cs^+	−1.43	1.10	1.39	3.86	1.13
$\lambda_{obs} = 550$ nm					
2	0.07	16.25	0.43	3.55	1.10
2 + H^+	0.32	16.19	0.18	4.28	1.08
2 + Na^+	0.14	16.63	0.31	3.86	1.24
2 + K^+	0.19	16.45	0.19	4.33	1.03
2 + Rb^+	0.25	24.20	0.16	3.55	1.06
2 + Cs^+	0.27	16.96	0.15	3.96	1.02

[a] Other statistical parameters (Durbin Watson, residual distribution, autocorrelation function) were found to be satisfactory.

Table 3. Kinetic parameters ($1/\lambda$) obtained from fluorescence emission decays of **2** (ca. 5×10^{-6} M) in the absence and in the presence of metal perchlorates (ca. 10^{-2} M) at 400 nm (monomer) and 550 nm (excimer) at −50 °C in degassed MeOH.

System	A_1	$1/\lambda_1$ [ns]	A_2	$1/\lambda_2$ [ns]	χ^2
$\lambda_{obs} = 400$ nm					
2	−0.47	1.11	0.42	10.52	1.03
2 + Na^+	−0.42	1.25	0.36	10.91	1.03
2 + K^+	0.01	2.34	0.04	10.40	1.16
2 + Rb^+	−1.07	1.76	0.93	10.09	1.13
2 + Cs^+	−0.82	1.92	0.72	10.70	1.15
$\lambda_{obs} = 550$ nm					
2	0.23	5.05	0.11	29.90	1.15
2 + Na^+	0.28	11.95	0.05	99.10	1.32
2 + K^+	−0.78	8.42	1.52	75.94	1.10
2 + Rb^+	−1.29	9.89	1.62	82.01	1.18
2 + Cs^+	−2.22	9.87	2.47	70.89	1.25

Although the experimental data fits well, it should be stated that such a scheme is an oversimplification for ligand **2** due to presence of several "monomer-like" emissions originating from either *cis* or *trans* ground-state conformations. However, a simplified kinetic scheme for the photophysical and photochemical properties of **2** has been proposed, from which rate constant parameters may be calculated, as described later (see Scheme 4 in Photochemistry Section).

At 20 °C, the $1/\lambda_2$ values are between 3–5 ns at both 400 nm and 550 nm. Therefore, these values, which are in the range of fluorescence lifetimes for 9-substituted anthracenes,[4d, 12] are ascribed to the *trans* species, which cannot generate intramolecular excimer for geometrical reasons. At 20 °C, the highest values of $1/\lambda$ found at 550 nm are probably due to the excimer formed by the intramolecular association of two anthracenes. These long lifetimes are not observed at 400 nm presumably because the intramolecular excimer does not revert to the monomer-like species (see Scheme 4: k_{MD} negligible). The lifetime shows a slight dependence on cation addition at 20 °C; thus, addition of Rb^+ gives rise to a significantly longer lifetime (24 ns) compared to 16 ns for other systems. The shortest values found at 400 nm which range from 0.59–2.34 ns may be attributed to the excited singlet anthracene (monomer-like species) that is responsible for the intramolecular excimer formation. At low temperature, as expected, a general increase in the kinetic parameters $1/\lambda$ is observed because the nonradiative deactivation channels (which usually need activation energy) are reduced (S → T transition, etc.). At 400 nm, the 1–2 ns decays correspond to the monomer species which leads to the excimer and the 10 ns values correspond to the monomer in the *trans* geometry which does not give the excimer. At 550 nm, the long lifetimes are assigned to the excimer contribution. A deeper investigation of these fluorescence decays would be necessary for a complete establishment of the kinetic scheme. Such a long study[4d] is outside the scope of this article.

Photochemistry: Upon irradiation at 368 nm with a xenon lamp, ligand **2** was found to be reactive in the presence or in the absence of cations, forming the cryptand **5** (Scheme 3) through the well-established [4π+4π] cycloaddition reaction of anthracene.[4e,f]

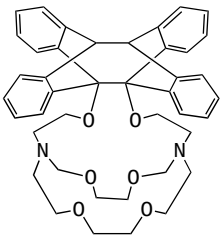

5

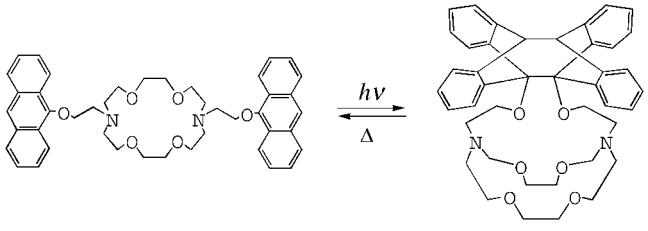

2 **5**

Scheme 3. The photochromic **2** ⇌ **5** process.

The intramolecular nature of this process was established by its efficiency being unaffected over the concentration range ($10^{-6}-10^{-4}$ M) and the fact that irradiation of compound **3** at the same concentrations gave no photoproduct. This cyclisation process is evidenced by the complete disappearance of the long wavelength absorption band (300–400 nm) in the UV spectrum that corresponds directly to the concentration of anthracene in solution (Figure 8). The formation of

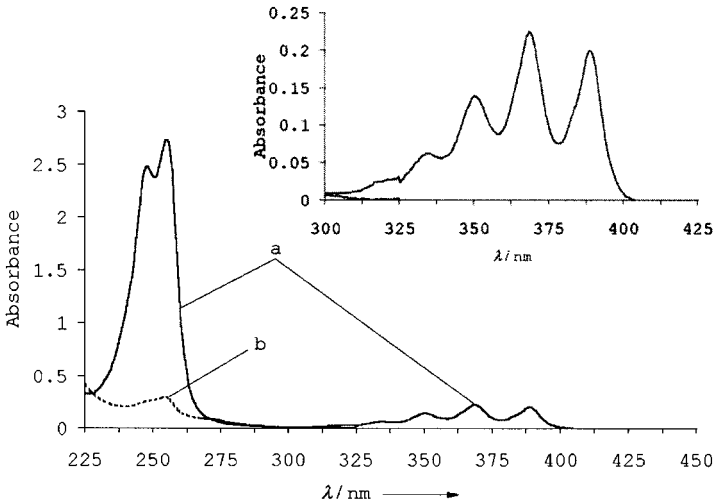

Figure 8. UV spectrum of crown **2** (ca. 5×10^{-5} M, 20 °C recorded a) before irradiation and b) after complete conversion to cryptand **5** by continuous irradiation ($\lambda_{exc}=368$ nm) in degassed MeOH. Inset: expansion of ^1L_a band.

the 9,9′-10,10-anthracene dimer was proven by ^{1}H NMR spectroscopy; resonances typical of an o-xylene group emerged at $\delta=6.9$ (12H) and 7.3 ppm (4H) and at the same time, the signals corresponding to the anthracenyl protons disappeared (Figure 9). It is probable that the doublet at $\delta=$ 7.3 ppm corresponds to the hydrogen atom on each benzene ring situated in closest proximity to the oxygen atoms, whilst the remaining aromatic protons give rise to the upfield multiplet (Figure 10). Significantly, a singlet ($\delta=4.55$ ppm, 2H) also appears which corresponds to the bridgehead protons on the anthracene photodimer.[4f] The appearance of this singlet and the simplicity of the aromatic region of the NMR spectrum is direct evidence for the formation of the symmetrical photodimer.

The cyclisation quantum yields (Φ_{RD}) for the **2** → **5** forward process were measured in the absence and in the presence of cations and in the case of Rb^+ and Cs^+, three different counteranions were tested in order to investigate any anion effect on the cyclisation efficiency (Table 4). It can be seen that the photocyclisation quantum yield is slightly influenced by the nature of the bound substrate. The highest quantum yield was observed for the free ligand ($\Phi_{RD}=0.11$). This value is much greater than those found for analogous processes with more sterically hindered systems.[4d,e] Introduction of cations into the system lowers the quantum yield, although the conformation of the crown complex (*cis* or *trans*) does not appear to significantly affect the efficiency of the forward process.

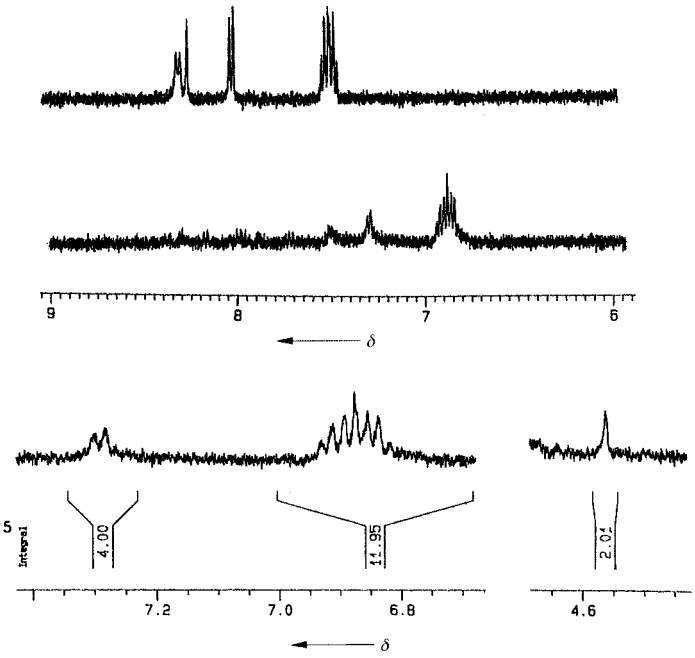

Figure 9. ^{1}H NMR spectrum (400 MHz) of ligand **2** (top) and cryptand **5** (middle) and expanded spectrum (bottom) showing integration and the singlet at $\delta=4.55$ ppm corresponding to the bridgehead protons, obtained in CD_3OD (3.5×10^{-4} M, 20 °C).

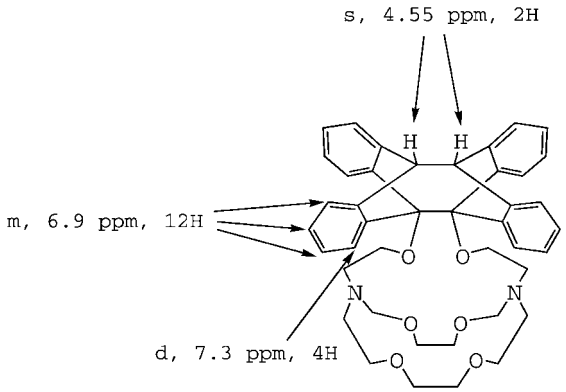

Figure 10. Proton assignment of cryptand **5** from ^{1}H NMR spectrurn in CD_3OD.

Table 4. Intramolecular photocycloaddition quantum yields ($\Phi_{RD}\pm10\%$) and rates of cycloaddition for the formation of **5** from **2** (ca. 5×10^{-5} M, 20 °C, $\lambda_{exc}=368$ nm) in the absence and in the presence of metal salts (ca. 10^{-2} M) in degassed MeOH.[a]

System	Φ_{RD} (368 nm)	k_{RD} [$\times10^{-6}$ s^{-1}][b]
2	0.11	9
2 + CF_3COOH	0.09	7.5
2 + $NaClO_4$	0.05	4.0
2 + $KClO_4$	0.08	6.5
2 + $RbClO_4$	0.07	3.8
2 + $RbNO_3$	0.07	–
2 + RbI	0.07	–
2 + $CsClO_4$	0.03	2.4
2 + $CsNO_3$	0.02	–
2 + CsI	0.02	–

[a] The reaction rates were calculated using single photon timing data and the reaction quantum yields as illustrated in Scheme 4. [b] k_{RD} is the reaction rate calculated from Equation (8) (see text and Experimental Section for details). The k_{RD} values are apparent rate constants, which do not take into account the *cis*/*trans* ratio.

  0947-6539/02/0815-3336 $ 20.00+.50/0 *Chem. Eur. J.* **2002**, *8*, No. 15

The largest drop in cyclisation efficiency occurs with the introduction of Cs^+ into the system. This is consistent with this cation being significantly larger than the macrocyclic cavity of the crown and consequently it sits above the plane of the ring, and hinders the cyclisation process. Steric hindrance would be reduced with Rb^+ due to its smaller size. This is borne out by the fact that $\pi-\pi$ stacking is more apparent in the Rb^+ complex, as described earlier. Even though these two cations enhance intramolecular excimer formation, they display poor quantum yields, as excimer formation requires an anthracene–anthracene separation distance of 3.0–3.3 Å, whereas for dimerisation to occur, the two aromatic rings must be within approximately 1.6 Å of one another,[4e,f, 12] and therefore are more dependent on the cation size. The relatively low quantum yield observed with Na^+ is consistent with the *trans* conformation of the complex being preferred with this ion.

As expected, the introduction of different counteranions into the system was found to have little or no effect on the cyclisation efficiency. The anions NO_3^- and I^- have no effect on the **2**/Rb^+ system, whilst with cesium a small reduction in the quantum yield is observed.

The rate constants for the forward **2** → **5** process (Table 4) were evaluated by using Scheme 4 and Equations (2)–(8). τ_M

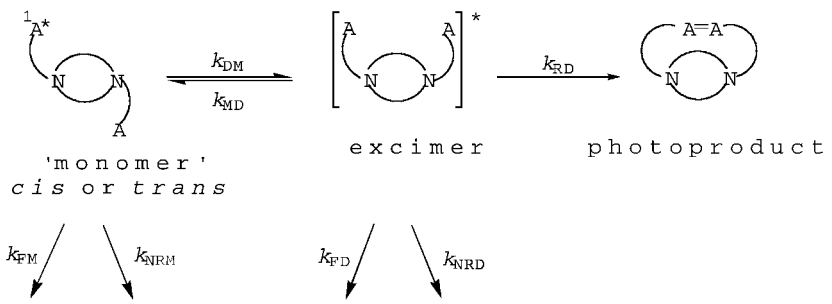

Scheme 4. Simplified kinetic scheme for the formation of cryptand **5** from crown ether **2**; A represents the anthracene ring; FM, NRM, DM, MD, FD, NRD, RD denote monomer fluorescence, monomer non-radiative deactivation, excimer formation from monomer, monomer formation from excimer, excimer fluorescence, excimer non-radiative deactivation, and reaction from excimer, respectively.

($1/\lambda_2$ values, Table 2, given at 400 nm and averaged to 4 ns) is assumed to be the singlet excited lifetime of the monomer species (*trans* isomer) *that does not form* the excimer. τ'_M ($1/\lambda_1$ values, Table 2, calculated at 400 nm and averaged to 1 ns) is assumed to be the lifetime of the monomer species (*cis* isomer) that *forms* the excimer (see Experimental Section for a worked example); k_D and τ_D are excimer rates of deactivation and excimer lifetime, respectively. τ_D is assumed to be equivalent to the $1/\lambda_1$ values (Table 2) at 550 nm that range from 16–24 ns (because no excimeric contribution was detected for the "monomer" decay, discarding the back process).

$$k_M = k_{FM} + k_{NRM} \quad (2)$$

$$\tau_M = 1/k_M \qquad (\tau_M = 1/\lambda_2 \text{ at } 400 \text{ nm}) \quad (3)$$

$$\tau'_M = 1/(k_M + k_{DM}) \qquad (\tau'_M = 1/\lambda_1 \text{ at } 400 \text{ nm}) \quad (4)$$

$$\tau_D = 1/k_D \qquad (\text{excimer lifetime}) \quad (5)$$

$$\tau_D = 1/(k_{FD} + k_{NRD} + k_{MD} + k_{RD}) \quad (6)$$

The rate constant for dimerisation (Φ_{RD}) is:

$$k_{RD} = \Phi_{RD}\left(\frac{k_M(k_D + k_{MD}) + k_D k_{DM}}{k_{DM}}\right) \quad (7)$$

The value of k_{MD} is negligible ($k_{MD} \ll k_D$), that is, there is no "back formation" of monomer from excimer (see Tables 2 and 3). Equation (7) then simplifies to :

$$k_{RD} = \Phi_{RD}\left(\frac{k_M k_D + k_D k_{DM}}{k_{DM}}\right) \quad (8)$$

The rate constants (k_{RD}) follow the same trend as the reaction efficiencies (Φ_{RD}) (Table 4). The free ligand displays the highest efficiency of dimerisation and the lowest values are observed for the **2**/Na^+ system (which is predominately *trans*) and the sterically hindering Rb^+ and Cs^+ complexes.

Thermal dissociation: When left in the dark or when heated, the cryptand **5** reverts back to the starting material **2** following first-order kinetics.[4f] This process can be monitored by the reappearance of the 300–400 nm component in the UV spectrum in MeOH and by the reappearance of the characteristic anthracenyl resonances in the ^1H NMR spectrum in CD_3OD. The thermal dissociation rate constants for the process **5** → **2** were evaluated[4d–f] in the absence and presence of an excess of H^+ and Group 1 metal salts (added as a solid) with different counteranions (Table 5). The stability of the photoproduct was found to be greater than that of other anthracene dimers,[4b,d,e, 13] as demonstrated by the slow dissociation rate of approximtaley $10^{-6}\,s^{-1}$ in most cases. The rate of dissociation was further stabilised by the addition of smaller Group 1 cations (Na^+, K^+), whereas the rate increased when the larger cations, Cs^+ and especially Rb^+, were added to the system.

It is likely that three major factors play a role in the rate of the reverse reaction:

Table 5. Thermal dissociation rate constants (**5** → **2**) (ca. 5×10^{-5} M) in the absence and in the presence of metal salts (ca. 10^{-2} M) recorded at 20 °C in MeOH.

System	k_{diss} [$\times 10^{-6}\,s^{-1}$]
2	3.4
2 + CF_3COOH	1.04
2 + $NaClO_4$	0.7
2 + $KClO_4$	2.3
2 + $RbClO_4$	170
2 + $CsClO_4$	8.5
2 + NaOAc	0.34
2 + RbOAc	250
2 + $RbNO_3$	255
2 + RbI	248
2 + $CsNO_3$	6.7
2 + CsI	7.2

Table 6. Fatigue of the system **2** ⇌ **5** (ca. 5×10^{-5} M, $\lambda_{exc} = 368$ nm) in the absence and in the presence of metal salts (ca. 10^{-2} M) after ten closing and opening cycles in degassed MeOH.

System	% decrease in absorbance at 368 nm
2	10
2 + CF_3COOH	13
2 + $NaClO_4$	23
2 + $KClO_4$	56
2 + $RbClO_4$	4
2 + $CsClO_4$	15

1) Strain in the C–C bonds of the cryptand/cryptate.
2) Oxygen lone pair repulsion in the cryptand/cryptate.
3) π – π interactions in the crown/coronate.

From the NMR studies it has been demonstrated that π – π stacking predominates in the Rb^+ and Cs^+ complexes of **2**. Such a stabilising interaction in the transition state would help to increase the opening rate in the presence of these two cations (see Scheme 5). However, for the caesium complex it is envisaged that a major contributing factor is the strain introduced into the cryptate due to the size of the metal ion. This is a less reasonable explanation for the rubidium system, however, as studies on related (but albeit less bulky) cryptands show that the metal fits within the spherelike cavity fairly comfortably.[14] The dramatic increase in the rate for the Rb^+ complex (ca. 100-fold relative to free **2**) is therefore more difficult to explain. One reason may be that the geometry of the Rb^+ cryptate is such that the oxygen lone pairs on the bulky aromatic arm are forced particulary close to one another to maximise coordination from the other donor atoms in the ligand. Such an interaction has previously been shown to be a contributing factor in the dissociation of related bis-anthracenes[4e, 13] and may therefore play a role in this system. Hence it is likely that for the Rb^+ complex, the combination of relative strain in the cryptate, oxygen lone pair-lone pair repulsion and a stabilised "π – π-like" transition state for the reopening process (NMR, UV and fluorescence studies indicate the most favourable π – π interaction and the most symmetrical and long-lived excimer in the Rb^+ complex), all contribute to the high k_{diss} value.

In contrast to the larger cations, Na^+ and K^+ slow down the rate of the opening process. A similar effect has been observed with other cyclic → linear systems.[4b,d,e] The smaller size of these cations probably allows for more flexibility in the system (compared to Rb^+ and Cs^+) and, therefore, the cryptate can arrange itself in such a way that oxygen lone-pair interactions are minimised. Any cation coordination by the two oxygen atoms in the bulky aromatic arm may also minimise such interations. The small degree of π – π stacking in the analogous crown complexes could also reduce the driving force for crown reformation.

When solutions of **2** were saturated with a range of different salts of a particular Group 1 metal, a moderate effect in the rate of thermal dissociation was observed (Table 5). For example, when sodium acetate was added, the rate of dissociation was half that observed with sodium perchlorate. However, in the **2**/Rb^+ cryptate, an increase in the rate constant (relative to the perchlorate) was observed when different counteranions were used. A small reduction in the rate constant was observed when different caesium salts were tested. It is most likely that these differences in rates are principally due to a solubility effect rather than to any anion effect, as best shown with the studies using the rubidium and sodium salts; addition of the more soluble (compared to $RbClO_4$) acetate, nitrate and iodide salts of rubidium result in a greater percentage of free ligand being complexed. As the dissociation rate constant is an average value of all complexed and uncomplexed species in solution, the rate therefore increases. The opposite effect is observed with sodium salts for which addition of sodium acetate results in an even greater decrease in the rate of dissociation, again due to increased solubility of the salt, and a greater percentage of complexed ligand in solution. This proves that the rate is not anion-dependent as, if it were, the observed effect (an increase or decrease in rate) would be the same for both Na^+ and Rb^+. This was confirmed by measuring k_{diss} for a particular metal cation with a range of counteranions, but each time using an *identical molar excess* (ca. 200-fold) of *dissolved* salt, resulting in almost identical rate constant values.

Fatigue studies: To examine the ability of the system to withstand the cyclisation process, solutions of **2** and its metal complexes were successively irradiated to form the cryptand **5** and then immediately heated to re-form the crown a total of ten times each. The concentration of anthracene present after ten cycles was obtained by examining the 300 – 400 nm band in the UV spectra. Each solution was found to have a decreased anthracene concentration with respect to the starting solution, which indicated that some decomposition had occurred (Table 6). Therefore, under these experimental conditions, this particular system undergoes too much fatigue to consider applications. However it is interesting to note that the percentage decrease for the Rb^+ complex is much less than that for the other complexes (Figure 11). Clearly, the ease at which the crown is reformed in the presence of this cation plays a role in stabilising the switching process and preventing fatigue.

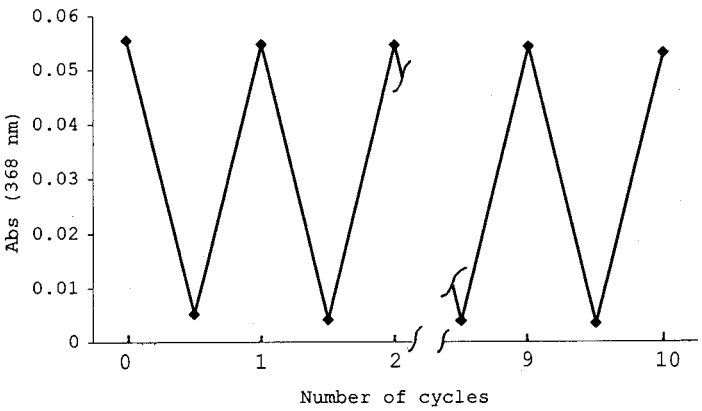

Figure 11. Reversibility of the system **2** ⇌ **5** (ca. 5×10^{-5} M, 20 °C $\lambda_{exc} =$ 368 nm) with $RbClO_4$ (ca. 10^{-2} M) in degassed MeOH through 10 successive closing and opening reactions (cycles 4 – 9 are omitted for clarity).

0947-6539/02/0815-3338 $ 20.00+.50/0 *Chem. Eur. J.* **2002**, *8*, No. 15

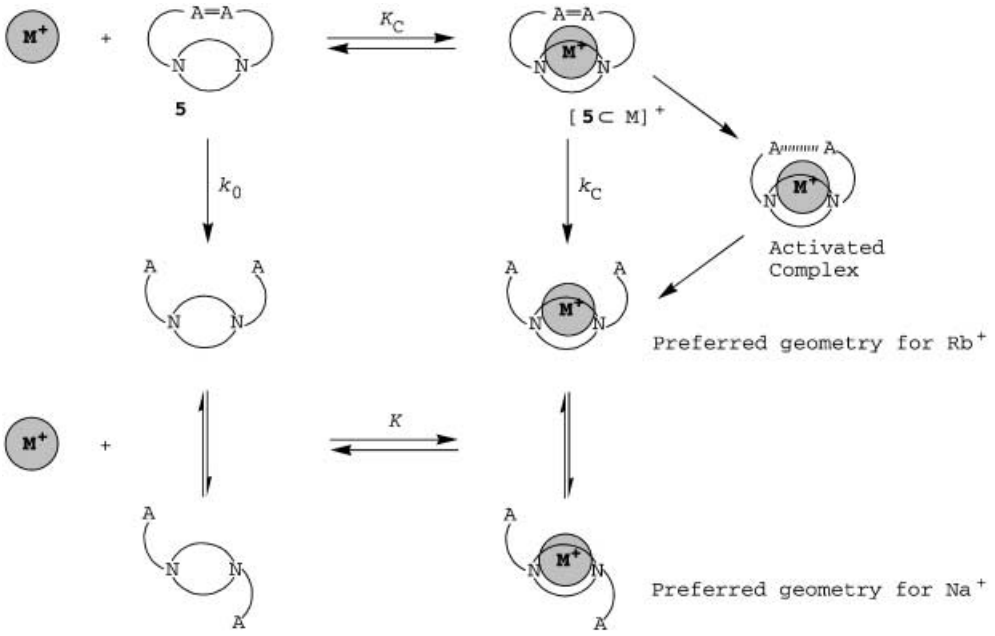

Scheme 5. Square scheme depicting the relationship between K, K_c k_o and k_c (see text for details).

Cation binding constants: To examine the effect of the photochromic process on cation binding strength, cation binding constants in methanol for the coronand **2** (K) and the cryptand **5** (K_c) have been evaluated. Scheme 5 depicts the relationship between K, K_c, k_o and k_c, in which k_o is the rate constant for the thermal dissociation of **5** to **2** ($3.4 \times 10^{-6}\,s^{-1}$, Table 5) and k_c is the analogous rate constant for a particular metal cation complex.

*Coronand **2***: Binding constants between **2** and alkali metal cations were determined in methanol with the LETAGROP program[15] by using UV or fluorescence spectroscopy. For the Na^+, K^+ and Cs^+ complexes, the values were obtained (Table 7) by monitoring changes to the second electronic transition band (^1B_b) of anthracene upon addition of aliquots of metal cation. In the case of the Rb^+ complex, changes to the monomer region of the fluorescence spectrum of **2** were monitored upon addition of cation.

Table 7. Cation binding constants in MeOH at 20 °C.

System	Method	$\log K$[a]
$[Na\subset \mathbf{2}]^+$	GS[b]	4.11
$[K\subset \mathbf{2}]^+$	GS[b]	5.85
$[Rb\subset \mathbf{2}]^+$	ES[c]	4.14
$[Cs\subset \mathbf{2}]^+$	GS[b]	3.42

[a] Error approximately 10%. [b] By UV spectroscopy (GS = ground state). [c] Obtained from fluorescence spectroscopy (ES = excited state, $\lambda_{exc} = 368$ nm), because the absorption spectra were observed not to undergo significant modifications in the presence of Rb^+.

The results show that the adoption of primarily a *cis* or a *trans* conformation does not affect the binding strength. However, changes in the pendant-arm proton resonance values on the NMR spectra and the general the *cis–trans* relationship described above indicate that the oxygen atom on each pendant arm does participate in binding. Furthermore, the binding constant values are similar to those quoted for other diaza-crown systems in which pendant-arm coordination takes place (e.g., **6**,[9] $\log K = 4.75$ with Na^+ and $\log K = 5.46$ with K^+ in methanol) and are greater than those quoted for systems with pendant arms containing no donor atoms (e.g., **7**,[16] $\log K = 2.84$ with Na^+ in methanol). As expected, the values follow simple size-match arguments, with K^+ the most strongly bound cation.

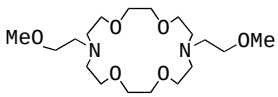

6

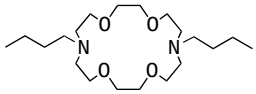

7

*Cryptand **5***: It has previously been shown by Shinkai[17a] that the cation binding constant can be determined kinetically for systems similar to the one described in Scheme 5 by using Equation (9), established previously by Connors and coworkers.[17b] This relationship is valid for the formation of a 1:1 complex under $[M^+] \gg [\mathbf{2}]$, in which k_{obs} is the observed rate constant at a particular concentration of cation $[M^+]$ and (K_c) is the binding constant for the cryptand, the equilibrium being established faster than the dissociation processes. Other parameters have been defined above, see Scheme 5.

$$\frac{k_0}{k_{obs} - k_0} = \left(\frac{k_0}{k_c - k_0}\right) + \left(\frac{k_0}{k_c - k_0}\right)\frac{1}{K_c}\frac{1}{[M^+]} \qquad (9)$$

From a plot of $k_o/k_{obs} - k_0$ against $1/[M^+]$, $k_o/k_c - k_0$ (intercept) and $(k_o/k_c\text{-}k_0)/K_c$ (slope) can be determined, allowing K_c and k_c to be calculated.

Results were obtained for a small (Na^+) and a large cation (Rb^+). k_{obs} was measured at least at four different concentrations of metal acetate salt and the results subjected to the mathematical treatment outlined above and plotted on a graph, (see Supporting Information for the system with Na^+). The resulting k_c and K_c values are as follows: $[\mathbf{5}{:}Na]^+$, $k_c = 0.90 \times 10^{-6}\,s^{-1}$, $\log K_c$ ($\pm 5\,\%$) = 1.68; $[\mathbf{5}{:}Rb]^+$, $k_c = 255 \times 10^{-6}\,s^{-1}$, $\log K_c$ ($\pm 5\,\%$) = 1.91.

The theoretical rate constants (k_c) are in fairly good agreement to those displayed in Table 5 (k_{diss}); once again, Na^+ is seen to slow the opening rate relative to the free ligand, whereas Rb^+ greatly enhances the rate. However, the values obtained for log K_c indicate that binding in the "closed" cryptand **5** is considerably weaker than the binding in the corresponding "open" crown ether **2**. This result is unexpected, since it is well known that, given the same number of donor atoms, the spherical and three-dimensional structure of a cryptand should make it a better ligand than its two-dimensional crown counterpart (the so-called macrocyclic effect[1a, 18]). However, in this case, whereas the cation binding affinity of **2** is as expected for a pendant arm system,[16] the introduction of a bulky aromatic group onto one arm of the [2.2.2]-cryptand drastically reduces the binding affinity (cf. for the complex [[2.2.2]-cryptand:$Na]^+$, $\log K = \sim 8.0$ in methanol[14]). It is interesting to note that a related cryptand **8**, containing an aromatic arm with donor atoms that are unable to bind cations strongly for steric reasons, also has a much lower binding affinity with Na^+ compared with [2.2.2]-cryptand ($\log K = 3.0$ in methanol).[19] It is therefore likely that the four benzene groups in **5** distort the ligand in such a way that the cation is prevented from strongly interacting with donor atoms in at least one arm of the cryptand cavity. In contrast, the bulky pendant arms of the crown ether **2** are flexible enough to orientate themselves in such a way that strong cation coordination is possible.

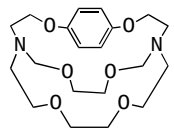

8

Conclusion

The **2**–**5** photochromic cation receptor is an effective iono-photoswitching system[1a] in which the binding affinity towards Group 1 cations is controlled in a reversible manner by light. The system also exhibits gated photochromism[1b] in that photochromism efficiency, in particular the rate of the thermal reverse reaction, is changed by metal cations. The considerable difference in cation binding strength between the two forms of over two orders of magnitude demonstrates how effective bis-anthracenyl photochromic systems are in bringing about large changes in ligand conformation and structure.

Experimental Section

General: The solvents and reagents were obtained from commercial suppliers and used without further purification. Anhydrous solvents were dried by the usual procedures and used directly. Preparation of all target compounds was carried out under an atmosphere of dry nitrogen. ^1H and ^{13}C NMR spectra were recorded on Bruker AC 300 or Bruker Avance 400 spectrometers. IR spectra were recorded on a Nicolet Magna 550 spectrometer. Elemental analyses were determined at the University of Exeter with a Carlo Erba EA 1110 elemental analyser. Mass spectra were measured by the EPSRC National Mass Spectrometry Service Centre at the University of Wales, Swansea with a Finnigan MAT 900 XLT spectrometer. Melting points (m.p.) were recorded on a Gallenkamp melting point apparatus and are uncorrected.

Spectroscopic grade solvents were used for the spectrophotometric measurements. A microbalance (Mettler ME 30, sensitivity 0.1 μg) was used to weigh samples for spectroscopic measurements. UV spectra: Hitachi U-3300 spectrophotometer or Unicam UV4 spectrometer. Fluorescence spectra: Hitachi F-4500. The fluorescence quantum yields were determined by comparison with quinine sulfate in 1 M sulfuric acid ($\Phi_F = 0.55$).[20] No fluorescent contaminants were detected upon excitation in the wavelength region of experimental interest. The experimental decay measurements were treated by using the Decan 1.0 program;[21a] the goodness of the fit was appreciated by inspection of χ^2 and other statistical parameters.[21b] The binding constants were calculated with the LETAGROP-SPEFO program.[15] The photocyclisation reactions were carried out by using a xenon lamp (2000 W) coupled with a monochromator and the reaction quantum yields were determined at $\lambda = 368$ nm by the Parker method (potassium ferrioxalate).[22] All fluorescence experiments and quantum yields measurements were performed on freeze-and-thaw degassed samples.

Kinetic scheme: Equation (8) (see text) was used to calculate k_{RD} at 20 °C.

k_M: This value was taken as the decay rate constant of the *trans* form which does not generate the excimer ($1/\lambda_2$, Table 2, averaged to 4 ns, so that $k_M = 2.5 \times 10^8\ s^{-1}$.

k_{DM}: One postulates that the *cis* form has the same kinetic parameters as the *trans* form in the absence of excimer formation which provides another deactivation channel; this leads to Equation (10):

$$k_{DM} = \lambda_1 - k_M \qquad (10)$$

$1/\lambda_1$ is postulated as the decay parameter of the *cis* form (no excimer dissociation to excited monomer), averaged to 1 ns, thus $k_{DM} = 7.5 \times 10^8\ s^{-1}$. For example, for the free ligand **2**:

$k_{RD} = 0.11 \times 6.15 \times 10^7 [(2.5 \times 10^8 + 7.5 \times 10^8)]/7.5 \times 10^8 = 9 \times 10^6\ s^{-1}$

X-ray crystallography: Crystals of **2** and $[\mathbf{2}{:}2H]^+$ were mounted in a random orientation on a glass wool fibre glued to a glass capillary. Combined phi and omega scans were performed at 150 K on a Nonius KappaCCD equipped with a Nonius FR591 rotating anode ($\lambda Mo_{K\alpha} = 0.71073$ Å). The structures were solved by direct methods, SHELXS-97[23] and refined with SHELXL-97.[24] Hydrogen atoms were included in the refinement, but were constrained to ride on the atom to which they are bonded. The data were corrected for absorption effects by using SORTAV.[25] Details of the structure refinement and data collection are presented in Table 8. CCDC-168107 and CCDC-168108 contain the supplementary crystallographic data for this paper. These data can be obtained free of charge via www.ccdc.cam.ac.uk/conts/retrieving.html (or from the Cambridge Crystallographic Data Centre, 12 Union Road, Cambridge CB2 1EZ, UK; fax: (+44) 1223-336-033; or e-mail: deposit@ccdc.cam.ac.uk).

Synthesis of 2 (Route 1)

4,13-Bis[2-(9-anthryloxy)ethyl]-4,13-diaza-[18]crown-6 (2): A mixture of 4,13-diaza-[18]crown-6 (0.4 g, 1.52 mmol), 9-(2-iodoethoxy)anthracene (1.33 g, 3.81 mmol) and iPr_2EtN (1.5 mL, 11 mmol) in anhydrous MeCN (60 mL) was heated at reflux under a nitrogen atmosphere for 72 h, cooled and concentrated in vacuo. The residue was then dissolved in CH_2Cl_2 (50 mL) and extracted with H_2O (3 × 50 mL). The organic phase was dried ($MgSO_4$) and the solvent removed under reduced pressure to give a brown oil, which was subjected to column chromatography on neutral alumina (CH_2Cl_2 with 1 % MeOH) to yield 0.34g (32 %) of the desired product as an orange semisolid which solidified upon prolonged drying. M.p. 111 °C; ^1H NMR ($CDCl_3$): $\delta = 3.02$ (t, $J = 6.0$ Hz, 8H; NCH_2), 3.24 (t, $J = 6.0$ Hz, 4H; NCH_2), 3.65 (s, 8H; OCH2), 3.72 (t, $J = 6.0$ Hz, 8H; OCH_2), 4.27 (t, $J = 6.0$ Hz, 4H; OCH_2), 7.44–7.48 (m, 8H; $C_{14}H_9$), 8.98 (d, $J = 4.6$ Hz, 4H;

  0947-6539/02/0815-3340 $ 20.00+.50/0 *Chem. Eur. J.* **2002**, *8*, No. 15

Table 8. Crystal data and collection parameters refinement for **2** and $[\mathbf{2}{:}2H]^{2+}$.

	2	$[\mathbf{2}{:}2H]^{2+}$
formula	$C_{44}H_{50}N_2O_6$	$C_{48}H_{52}F_6N_2O_{11}$
M_r	702.86	946.92
crystal system	monoclinic	triclinic
space group	$P2_1/c$	$P\bar{1}$
a [Å]	10.579(2)	11.3520(10)
b [Å]	17.772(4)	12.8940(10)
c [Å]	10.1254(16)	17.2230(10)
α [°]	90	68.610(10)
β [°]	93.545(6)	83.130(10)
γ [°]	90	80.130(10)
V [Å^3]	1900.0(6)	2308.1(3)
ρ_{calcd} [Mg m^{-3}]	1.229	1.362
μ [mm^{-1}]	0.081	0.112
crystal size [mm]	$0.2 \times 0.1 \times 0.05$	$0.2 \times 0.15 \times 0.1$
θ range [°]	2.94–23.26	2.16–27.47
reflections collected/unique	5590/2269	75082/10535
R_{int}	0.2052	0.0630
data/restraints/parameters	2269/0/236	10535/0/622
final R indices $[I > 2\sigma(I)]$ $R1/wR2$	0.0788/0.1280	0.0616/0.1749
R indices (all data) $R1/wR2$	0.3258/0.1988	0.0905/0.1905
$\rho_{max}\rho_{min}$ [e Å^{-3}]	0.164/−0.185	0.605/−0.703

$C_{14}H_9$), 8.20 (s, 2H; $C_{14}H_9$), 8.35 (d, $J = 3.6$ Hz, 4H; $C_{14}H_9$); ^{13}C NMR ($CDCl_3$): $\delta = 54.85, 55.93, 70.27, 70.84, 74.36, 122.05, 122.58, 124.69, 125.09, 125.45, 128.37, 132.43, 151.38$; IR (KBr 1%): $\tilde{\nu} = 3050, 2950, 2880, 2820, 1625, 1340, 1135, 1105, 1070, 935, 740$ cm^{-1}. elemental analysis calcd (%) for $C_{44}H_{50}N_2O_6$: C 75.19, H 7.17, N 3.98; found: C 75.43, H 7.17, N 3.93; MS (FAB): m/z calcd for $C_{44}H_{51}N_2O_6$: 703.3747; found 703.3780 [M^++H]; MS (FAB$^+$/Na$^+$): m/z (%): 725 (100) [M^++Na], 703 (52) [M^++H].

1-[2-(9-Anthryloxy)ethyl]-1-aza-[18]crown-6 (3): A mixture of 1-aza-[18]crown-6 (0.3 g, 1.14 mmol), 9-(2-iodoethoxy)anthracene (0.4 g, 1.14 mmol) and iPr$_2$EtN (1 mL, 7.7 mmol) in anhydrous MeCN (40 mL) was heated at reflux under a nitrogen atmosphere for 48 h. The mixture was cooled and concentrated in vacuo and the residue then dissolved in CH_2Cl_2 (50 mL) and extracted with H_2O (3×50 mL). The organic phase was dried ($MgSO_4$) and the solvent removed under reduced pressure to give a brown oil, which was subjected to column chromatography on neutral alumina (CH_2Cl_2 with 1% MeOH) to yield 0.38g (68%) of the desired product as a brown sticky oil. ^{1}H NMR ($CDCl_3$): $\delta = 3.1$ (t, $J = 5.6$ Hz, 4H; NCH_2), 3.25 (t, $J = 6.2$ Hz, 2H; NCH_2), 3.7 (t, $J = 5.6$ Hz, 20H; OCH_2), 4.3 (t, $J = 6.2$ Hz, 2H; OCH_2), 7.5 (m, 4H; $C_{14}H_9$), 8.00 (d, $J = 6$ Hz, 2H; $C_{14}H_9$), 8.25 (s, 1H; $C_{14}H_9$), 8.35 (d, $J = 6$ Hz, 2H; $C_{14}H_9$); ^{13}C NMR ($CDCl_3$, 100 MHz): $\delta =$ 54.91, 55.95, 70.27, 70.53, 70.69, 70.84, 71.01, 74.36, 122.18, 122.51, 124.62, 125.20, 125l.47, 128.39, 132.40, 151.36; MS (FAB): m/z calcd for $C_{28}H_{38}NO_6$: 484.2747 [M^++H]; found: 484.2692.

Syntheses of 2 (Route 2)

Ethyl-9-anthryloxyacetate (9): Anthrone (5 g, 0.025 mol), K_2CO_3 (50 g, 0.36 mol) and freshly distilled (over K_2CO_3) acetone (100 mL) under nitrogen bubbling were placed in a round-bottomed flask equipped with a reflux condenser, a pressure equalizing dropping funnel and a stirrer. A bright orange colour developed under stirring and ethylchloroacetate (13 mL, 0.12 mol) in acetone (50 mL) was added; the mixture was refluxed for 4 h. The pale yellow medium was hydrolysed and acidified. After usual work up, the dried organic phase (CH_2Cl_2) was purified by chromatography on silica (eluent: CH_2Cl_2) to provide a yellow pasty solid, 4.15 g (yield 57%) identified to **9** and used without further purification. ^{1}H NMR ($CDCl_3$): $\delta = 1.1$ (t, $J = 10$ Hz, 3H; CH_3), 4.1 (q, $J = 10$ Hz, 2H; CH_2-CH_3), 4.5 (s, 2H; O-CH_2-CO), 7.1–8.3 (m, 9H; Ar); IR (neat): $\tilde{\nu} = 3060, 3020, 2950, 2900, 2880, 2840, 1765, 1735, 1600, 1430, 1400, 1330, 1270, 1200, 1100, 1030, 870, 830, 780, 730$ cm^{-1}.

9-Anthryloxyacetic acid (10): The above ester **9** (4.6 g, 1.64 mmol) was heated with a solution of KOH (10 g, 0.178 mol) in EtOH (150 mL) for 3 h. After solvent evaporation, the residue was poured on ice, acidified, filtered and dried, providing **10** as a white powder, 1.75 g (42%). M.p. ≈90 °C; ^{1}H NMR (DMSO): $\delta = 4.9$ (s, 2H; O-CH_2-CO), 7.5–8.4 (m, 9H; Ar); 13 (br d, 1H; COO*H*); IR (KBr): $\tilde{\nu} = 3600-2400$ (br s, characteristic of COOH), 1710 (s), 1420, 1400, 1330, 1250, 1100, 850, 700 cm^{-1}. MS (EI): m/z (%): 252 (26) [M^+], 193 (100).

9-Anthryloxyacetic acid chloride (11): The carboxylic acid **10** (1.95 g, 7.74 mmol) dissolved in benzene (200 mL) was refluxed in the presence of oxalyl chloride (15 mL, 0.17 mol) for 3 h. After evaporation of the volatile materials, the residue (2 g) was used without further purification. IR (KBr): $\tilde{\nu} = 1800$ (s, C=O), 1620, 1340 (s), 1110 (s), 940, 920, 780, 760, 730 cm^{-1}.

4,13-bis(9-anthryloxyacetyl)-4,13-diaza-[18]crown-6 (12): A solution of 4,13-diaza-[18]crown-6 (0.97 g, 3.7 mmol) in benzene (100 mL) was added dropwise under nitrogen bubbling to a solution of triethylamine (7.4 g, 73 mmol) and acid chloride **11** (2 g, 7–4 mmol) in benzene (120 mL). The mixture was mixed with an 0.1M sodium hydroxide aqueous solution (100 mL) and stirred for 15 minutes. The benzene was evaporated under reduced pressure and the organic phase was extracted with CH_2Cl_2, neutralized, washed and dried. The crude product (1.8 g) was separated by chromatography on alumina to collect **12** (1 g, 37%), which was used for the following step without further purification. ^{1}H NMR ($CDCl_3$): $\delta = 3.4-3.8$ (m, 24H; CH_2-CH_2O), 4.9 (s, 4H; O-CH_2-CO), 7.3–8.5 (m, 18H; Ar). IR (neat): $\tilde{\nu} = 3060, 3020, 2950, 2910, 2880, 1670, 1360, 1140, 1100, 1040, 920, 750$ cm^{-1}. MS (FAB$^+$): m/z (%): 753 (50) [M^++Na], 731 (39) [M^++H].

4,13-Bis[2-(9-anthryloxy)ethyl]-4,13-diaza-[18]crown-6 (2): A solution of diamide **12** (600 mg, 0.82 mmol) in THF (50 mL) placed in a round-bottomed flask equipped with a reflux condenser and a serum cap, was cooled to 0 °C. Then B_2H_6 (15 mL, 1M solution in THF) was added with a syringe and the mixture was refluxed under stirring for 2 h. After cooling to ambient temperature, the excess diborane was quenched with water (20 mL), added cautiously. The organic solvent was evaporated and the solid filtrated dried and suspended in THF (≈100 mL). Trifluoroacetic acid (35 mL) was slowly added and the medium was refluxed for 2 h; it was then made basic (pH ≈ 10) by addition of Et_4NOH (20%). After extraction by CH_2Cl_2 followed by usual workup the crude product was crystallized in benzene/heptane to pale yellow crystals. M.p. 114 °C (288 mg, 50%). The spectroscopic characteristics of this product were found to be identical to those of the product prepared by Route 1.

Formation of photocycloisomer 5

Method 1: Compound **2** was dissolved in CD_3CN (10^{-4}M) in an NMR tube immersed in a water-containing Pyrex vessel and irradiated with a high-pressure mercury lamp. The progress of the reaction was followed by UV spectroscopy (see Figure 8).

Method 2: Compound **2** was dissolved in CH_3OH in a UV cell (5×10^{-5}M) and irradiated with a monochromatic light (368 nm) to determine the reaction quantum yield (disappearance of **2** at $\lambda = 368$ nm).

No attempt was made to isolate and store the photoproduct whose half-lifetime is approximately 55 h at room temperature.

Acknowledgement

We thank the Engineering and Physical Sciences Research Council (EPSRC) for the award of a project studentship grant (to GM). We are grateful to the CNRS and the "Région Aquitaine" for financial support and indebted to J. Lauret, M. Gotta and Tran Thanh Hung Linh for technical assistance.

[1] a) J. M. Lehn, *Supramolecular Chemistry—Concepts and Perpectives*, VCH, Weinheim, **1995**; b) "Photochromism: Memories and Switches": *Chem. Rev.* **2000**, *100*, 1683–1890; c) *Photochromism, Molecules and Systems* (Eds.: H. Dürr, H. Bouas-Laurent), Elsevier, Amsterdam, **1990**, Chapter 14; d) *Organic Photochromic and Thermochromic Compounds*, *Vol. 2* (Eds.: J. C. Crano, R. J. Guglielmetti), Kluwer Academic/Plenum, New York, **1999**; e) "Organic Photochromism, IUPAC Technical Report": H. Bouas-Laurent, H. Dürr, *Pure Appl. Chem.* **2001**, *73*, 639–665.

[2] For other recent examples of crown-ether-based photochromic systems, see: a) M. Inouye, K. Akamatsu, H. Nakazumi, *J. Am. Chem. Soc.* **1997**, *119*, 9160–9165; b) K. Kimura, R. Mizutani, M. Yokoyama, R. Arakawa, Y. Sakurai, *J. Am. Chem. Soc.* **2000**, 122, 5448–5454;

c) O. A. Fedorova, S. P. Gromov, Y. V. Pershina, S. S. Sergeev. Y. P. Strokach, V. A. Barachevsky, M. V. Alfimov, G. Pèpe, A. Samat, R. Guglielmetti, *J. Chem. Soc. Perkin Trans. 2* **2000**, 563 – 570.

[3] J. M. Endtner, F. Effenberger, A. Hartschuh, H. Port, *J. Am. Chem. Soc.* **2000**, *122*, 3037 – 3046 and references therein.

[4] a) J. P. Desvergne, H. Bouas-Laurent, *J. Chem. Soc. Chem. Commun*. **1978**, 403 – 404; b) G. McSkimming, J. H. R. Tucker, H. Bouas-Laurent, J. P. Desvergne, *Angew. Chem*. **2000**, *112*, 2251 – 2153; *Angew. Chem. Int. Ed*. **2000**, *39*, 2167 – 2169; c) J. H. R. Tucker, H. Bouas-Laurent, P. Marsau, S. W. Riley, J. P. Desvergne, *Chem. Commun*. **1997**, 1165 – 1166 d) D. Marquis, J. P. Desvergne, H. Bouas-Laurent, *J. Org. Chem*. **1995**, *60*, 7984 – 7996; e) H. Bouas-Laurent H, A. Castellan, J. P. Desvergne, R. Lapouyade, *Chem. Soc. Rev*. **2001**, *30*, 248 – 263; f) H. Bouas-Laurent H, A. Castellan, J. P. Desvergne, R. Lapouyade, *Chem. Soc. Rev*. **2000**, *29*, 43 – 55.

[5] a) G. Deng, T. Sakaki, K. Nakashima, S. Shinkai, *Chem. Lett*. **1992**, 1287 – 1290; b) A. Beyeler, P. Belser, L. De Cola, *Angew. Chem*. **1997**, *109*, 2878 – 2881; *Angew. Chem. Int. Ed. Engl.* **1997**, *36*, 2779 – 2781; c) T. Jin, *Chem. Commun*. **2000**, 1379 – 1380.

[6] W. H. Pirkle, J. M. Finn, *J. Org. Chem*. **1983**, *48*, 2779 – 2880.

[7] N. Su, J. S. Bradshaw, X. X. Zhang, H. Song, P. B. Savage, G. Xue, K. E. Krakowiak, R. M. Izatt, *J. Org. Chem.* **1999**, *64*, 8855 – 8861.

[8] J. P. Desvergne, H. Bouas-Laurent, *Isr. J. Chem*. **1979**, *18*, 220 – 226.

[9] a) G. W. Gokel, *Chem. Soc. Rev*. **1992**, *21*, 39 – 47; b) S. L. De Wall, E. S. Meadows, L. J. Barbour, G. W. Gokel, *Chem. Commun.* **1999**, 1553 – 1554 and references therein.

[10] D. Wang, Y. Ge, H. Hu, K. Yu , Z. Zhou, *J. Chem. Soc. Chem. Commun.* **1991**, 685 – 687.

[11] J. Ferguson, A. Castellan, J. P. Desvergne, H. Bouas-Laurent, *Chem. Phys. Lett*. **1981**, *78*, 446 – 450 and references therein.

[12] J. B. Birks, *Photophysics of Aromatic Molecules*, Wiley, Chichester, **1970**, pp. 328 – 331.

[13] H. Bouas-Laurent, J. P. Desvergne, F. Fages, P. Marsau in *Frontiers in Supramolecular Organic Chemistry and Photochemistry* (Eds.: H. J. Schneider, H. Dürr), VCH, **1991**.

[14] R. M. Izatt, K. Pawlak, J. S. Bradshaw, R. L. Bruening, *Chem. Rev.* **1991**, *91*, 1721 – 1785 and references therein.

[15] a) L. G. Sillen, B. Warnquist, *Ark. Kemi*. **1968**, *31*, 315 – 339; b) L. G. Sillen, B. Warnquist, *Ark. Kemi*. **1968**, *31*, 377 – 390.

[16] V. J. Gatto, K. A. Arnold, A. M. Viscariello, S. R. Miller, C. R. Morgan, G. W. Gokel, *J. Org. Chem*. **1986**, *51*, 5373 – 5384.

[17] a) S. Shinkai, Y. Honda, K. Ueda, O. Manabe, *Bull. Chem. Soc. Jpn*. **1984**, 57, 2144 – 2149; b) J. A. Mollica, Jr, K. A. Connors, *J. Am. Chem. Soc*. **1967**, *89*, 308 – 317.

[18] H. K. Frensdorff, *J. Am. Chem. Soc*. **1971**, *93*, 600 – 606.

[19] E. Chapoteau, B. P. Czech, A. Kumar, A. Pose, *J. Inclusion Phenom.* **1988**, *6*, 41 – 47.

[20] W. H. Melhuish, *J. Phys. Chem*. **1961**, *65*, 229 – 235.

[21] a) T. de Roeck, N. Boens, J. Dockx, DECAN 1.0, Leuven (Belgium), **1991**; b) D. V. O'Connor, D. Phillips, *Time-Correlated Single Photon Counting*, Academic Press, London, **1984**.

[22] a) C. G. Hatchard, C. A. Parker, *Proc. R. Soc. London Ser. A*. **1956**, *235*, 518 – 536; b) C. G. Hatchard, C. A. Parker, *J. Phys. Chem*. **1959**, *63*, 22 – 26.

[23] G. M. Sheldrick, SHELXS-97, program for crystal structure solution, University of Göttingen, Germany, **1997**.

[24] G. M. Sheldrick, SHELXL-97, program for crystal structure refinement, University of Göttingen, Germany, **1997**.

[25] a) R. H. Blessing, *Acta Crystallogr. Sect. A* **1995**, *51*, 33 – 37; b) R. H. Blessing, *J. Appl. Crystallogr*. **1997**, *30*, 421 – 426.

Received: November 9, 2001
Revised: March 26, 2002 [F3676]

  0947-6539/02/0815-3342 $ 20.00+.50/0